arXiv:1612.05428v1 [hep-ph] 16 Dec 2016

Stability of Azimuthal-angle Observables under Higher Order Corrections in Inclusive Three-jet Production

F. Caporale[1], F. G. Celiberto[1,2], G. Chachamis[1],
D. Gordo Gómez[1*], A. Sabio Vera[1]

[1] Instituto de Física Teórica UAM/CSIC, Nicolás Cabrera 15
& Universidad Autónoma de Madrid, E-28049 Madrid, Spain.
[2] Dipartimento di Fisica, Università della Calabria &
Istituto Nazionale di Fisica Nucleare, Gruppo Collegato di Cosenza,
I-87036 Arcavacata di Rende, Cosenza, Italy.

December 19, 2016

Abstract

Recently, a new family of observables consisting of azimuthal-angle generalised ratios was proposed in a kinematical setup that resembles the usual Mueller-Navelet jets but with an additional tagged jet in the central region of rapidity. Non-tagged minijet activity between the three jets can affect significantly the azimuthal angle orientation of the jets and is accounted for by the introduction of two BFKL gluon Green functions. Here, we calculate the, presumably, most relevant higher order corrections to the observables by now convoluting the three leading-order jet vertices with two gluon Green functions at next-to-leading logarithmic approximation. The corrections appear to be mostly moderate giving us confidence that the recently proposed observables are actually an excellent way to probe the BFKL dynamics at the LHC. Furthermore, we allow for the jets to take values in different rapidity bins in various configurations such that a comparison between our predictions and the experimental data is a straightforward task.

*'La Caixa'-Severo Ochoa Scholar.

1 Introduction

One of the most active fields of research in Quantum Chromodynamics (QCD) is the resummation of large logarithms in the center-of-mass energy squared s for processes dominated by the so-called multi-Regge kinematics (MRK). To account for these logarithms, one can make use of the Balitsky-Fadin-Kuraev-Lipatov (BFKL) framework in the leading logarithmic (LLA) [1, 2, 3, 4, 5, 6] and next-to-leading logarithmic (NLLA) approximation [7, 8]. In inclusive multi-jet production, when the outermost in rapidity jets have a large rapidity difference, we may assume that the process follows the MRK and therefore, the BFKL resummation becomes relevant.

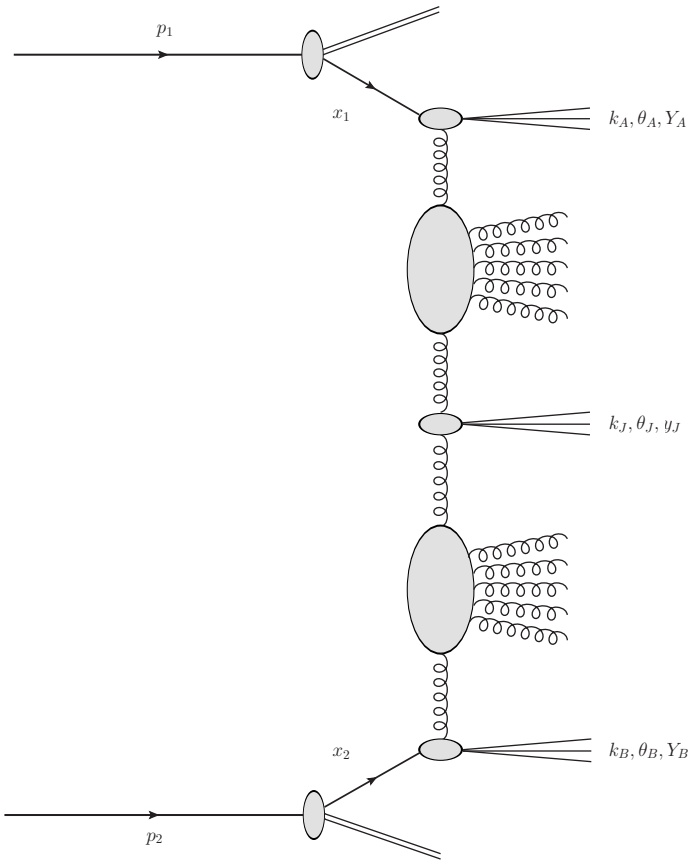

Figure 1: Inclusive three-jet production process in multi-Regge kinematics.

A classic example is Mueller-Navelet jets [9], that is, the configuration in hadronic colliders with two final state jets[1] which are produced with

[1] Another interesting idea, suggested in [10] and investigated in [11], is the study of the

large and similar transverse momenta, $k_{A,B}$, and a large rapidity separation $Y = \ln(x_1 x_2 s/(k_A k_B))$. $x_{1,2}$ are the longitudinal momentum fractions of the partons that are adjacent to the jets. Various works [12, 13, 14, 15, 16, 17, 18, 19, 20, 21, 22, 23, 24, 25, 26] addressing the azimuthal[2] angle (θ) profile of the two tagged jets, suggest the presence of important minijet activity populating the rapidity interval which can be taken into account by considering a BFKL gluon Green function connecting the two jets. However, it was shown that the azimuthal angle behaviour of the tagged jets is strongly contaminated by collinear effects [27, 28], that have their origin at the $n = 0$ Fourier component in θ of the BFKL kernel. This dependence is mostly canceled if ratios of projections on azimuthal angle observables $\mathcal{R}_n^m = \langle \cos(m\,\theta)\rangle / \langle \cos(n\,\theta)\rangle$ [27, 28] (where m, n are integers and θ is the azimuthal angle between the two tagged jets) are studied. It also seems that these offer a clearer signal of BFKL effects than the usual predictions for the behaviour of the hadron structure functions $F_{2,L}$ (well fitted within NLL approaches [29, 30]). The confrontation of different NLLA calculations for these ratios $\mathcal{R}_n^m$ [31, 32, 33, 34, 35] against experimental data at the LHC has been successful.

Recently, we proposed new observables for processes at the LHC that may be considered as a generalisation of the Mueller-Navelet jets. These processes are inclusive three-jet [36, 37] and four-jet production [38, 39] with the outermost jets widely separated in rapidity Y, whereas any other tagged jet is to be found in more central regions of the detector. The main idea behind all this effort is that we need more exclusive final states in order to be able to address a number of theoretical issues, *e.g.* what is the optimal way to implement the running of the strong coupling or could one speak about saturation effects at present energies, etc.

Investigating more exclusive final states (with more than two jets) although more challenging on a technical level, allows for more complex observables to be defined so that one can finally choose those that encapsulate the essence of these features of MRK that are distinct in the BFKL dynamics only. In the remaining of this paper, we will focus only on inclusive three-jet production.

---

production of two charged light hadrons, $\pi^{\pm}$, $K^{\pm}$, p, $\bar{p}$, with large transverse momenta and well separated in rapidity.

[2] In this work, we denote the azimuthal angles by θ contrary to the usual practice that prefers ϕ.

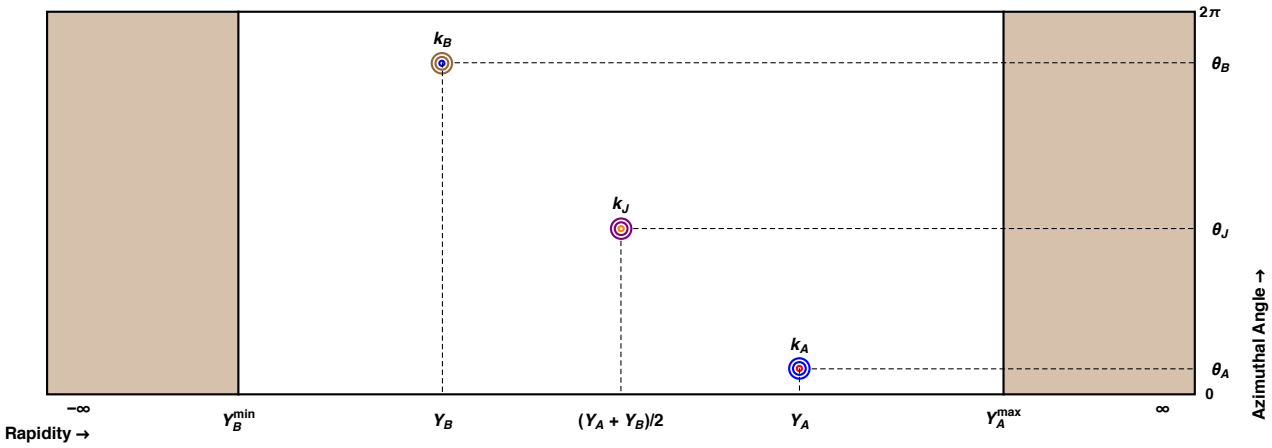

Figure 2: A primitive lego plot depicting a three-jet event. k_A is a forward jet with large positive rapidity Y_A and azimuthal angle θ_A, k_B is a forward jet with large negative rapidity Y_B and azimuthal angle θ_B and k_J is a central jet with rapidity y_J and azimuthal angle θ_J. The fade-brown areas to the left and right highlight the regions in rapidity that are not covered by the standard detectors.

The key idea presented in [36] was to get theoretical predictions for the partonic-level ratios

$$\mathcal{R}_{PQ}^{MN} = \frac{\langle \cos(M\,\theta_1)\cos(N\,\theta_2)\rangle}{\langle \cos(P\,\theta_1)\cos(Q\,\theta_2)\rangle}\,, \tag{1}$$

where θ_1 is the azimuthal angle difference between the first and the second (central) jet, while, θ_2 is the azimuthal angle difference between the second and the third jet.

In [37], we presented a first phenomenological analysis at LLA for the respective hadronic-level ratios R_{PQ}^{MN}. These were obtained after using collinear factorization to produce the two most forward/backward jets and convoluting the partonic differential cross section, which follows the BFKL dynamics, with collinear parton distribution functions included in the forward "jet vertex" [41, 42, 43, 44, 45, 46, 47]. In addition, the two Mueller-Navelet jet-vertices were linked with the centrally produced jet via two BFKL gluon Green functions. Finally, we integrated over the momenta of all produced jets, using actual LHC experimental cuts.

Our predictions in [37], although may in principle be directly compared to experimental data once these are available, do not resolve two issues: (I) They do not offer any estimate of the theoretical uncertainty that comes into play once higher order corrections are considered. (II) Since we restricted the central jet to be produced in the middle of the rapidity interval between the outermost jets, one could possibly raise concerns of whether a experimental

analysis following the kinematical setup used in Ref. [37] is possible at all. Here, we address both of these issues.

To that end, regarding issue (I), one needs to calculate higher order corrections for the ratios at partonic-level. This comprises of two steps: considering NLLA corrections to the BFKL kernel and NLO corrections to the jet vertices. However, although the corrections to the jet vertices may be in general significant, we expect them not to affect much the azimuthal angle characteristics of the jets which are driven mostly by the minijet activity in the rapidity intervals between the jets. Demanding three tagged jets along with central minijets leaves little room for higher order real emission activity near the jet vertices. We expect that the higher order virtual corrections to the vertices may be interpreted as K-factor corrections which would cancel out in our observables since we consider ratios. We have argued previously that the minijet activity is accounted for by the introduction of the two gluon Green functions. Large corrections from LLA to NLLA for the gluon Green function, which is actually a usual outcome in many BFKL-based calculations, could potentially have a strong impact on the ratios and this at any rate needs to be assessed. Therefore, in this work we work with NLLA[3] gluon Green functions and LO jet vertices.

The answer to issue (II) is, naturally, positive since allowing for the central jet to live in a rapidity range instead of a single point, as long as this range is located generally in the middle of the rapidity interval between the outermost jets, does not affect the values of the generalised rations in Eq. 1, as was shown in [36]. Nevertheless, to avoid any confusion and to have a complete study, in the present work we are also considering cases in which the central jet lives in a rapidity bin of unit width, while the central value of the bin may vary.

Other potential sources of uncertainty could be due to the particular PDF sets one uses. One can still argue though that the uncertainty due to different PDF sets does not need to be ascertained before one has gauged how large are the full beyond the LLA corrections to the partonic-level ratios, since it will be overshadowed by the latter. Indeed, from first tries we see no significant difference in the results when we work with different PDF sets and therefore we do not offer any dedicated analysis on that here.

In the bulk of the paper we present theoretical predictions for the ratios R_{PQ}^{MN} at NLLA and we compare these to the LLA ones. In particular, in Section 2 we define the computational framework and our notation for the LLA and NLLA calculations. In Section 3 we present results for R_{22}^{12}, R_{33}^{12} and R_{33}^{22} as a function of the rapidity distance Y between the outermost jets while the central jet is fixed at the middle of this distance, for both $\sqrt{s} = 7$ and $\sqrt{s} = 13$ TeV colliding energies. In Section 4, we present the LLA

[3]Note that from now on, we will refer to the results with NLLA gluon Green functions and LO vertices as NLLA results.

and NLLA results for R^{12}_{22}, R^{12}_{33} and R^{22}_{33} while the central jet is allowed to take values in the rapidity bin $[-0.5, 0.5]$. The results are plotted again as functions of the rapidity interval Y between the outermost jets for $\sqrt{s} = 7$ and $\sqrt{s} = 13$ TeV. In Section 5, we do not keep Y fixed at any certain value, instead, we allow for the forward jet to be in the rapidity interval $[3, 4.7]$, for the backward one to be in the symmetric rapidity interval $[-4.7, -3]$ while the rapidity of the central jet takes again values in a bin of unit 1. The central value of the bin though, may now take five different values, namely, $\{-1, -0.5, 0, 0.5, 1\}$ and we plot both the LLA and NLLA results for R^{12}_{22}, R^{12}_{33} and R^{22}_{33} as a function of that central value, again for $\sqrt{s} = 7$ and $\sqrt{s} = 13$ TeV. We finish our work with Conclusions and Outlook.

2 Hadronic inclusive three-jet production in multi-Regge kinematics

The process under investigation (see Figs. 1 and 2) is the production of two forward/backward jets, both characterized by high transverse momenta $\vec{k}_{A,B}$ and well separated in rapidity, together with a third jet produced in the central rapidity region and with possible associated minijet production. This corresponds to

$$\text{proton}(p_1) + \text{proton}(p_2) \to \text{j}(k_A, Y_A) + \text{j}(k_J, y_J) + \text{j}(k_B, Y_B) + \text{minijets} \ , \quad (2)$$

where $\text{j}(k_A, Y_A)$ is the forward jet with transverse momentum k_A and rapidity Y_A, $\text{j}(k_B, Y_B)$ is the backward jet with transverse momentum k_B and rapidity Y_B and $\text{j}(k_J, y_J)$ is the central jet with transverse momentum k_J and rapidity y_J.

In collinear factorization the cross section for the process (2) reads

$$\frac{d\sigma^{3-\text{jet}}}{dk_A\, dY_A\, d\theta_A\, dk_B\, dY_B\, d\theta_B\, dk_J\, dy_J d\theta_J} = \sum_{r,s=q,\bar{q},g} \int_0^1 dx_1 \int_0^1 dx_2 \ f_r\left(x_1, \mu_F\right) \ f_s\left(x_2, \mu_F\right) \ d\hat{\sigma}_{r,s}\left(\hat{s}, \mu_F\right) \ , \quad (3)$$

where the r, s indices specify the parton types (quarks $q = u, d, s, c, b$; antiquarks $\bar{q} = \bar{u}, \bar{d}, \bar{s}, \bar{c}, \bar{b}$; or gluon g), $f_{r,s}\left(x, \mu_F\right)$ are the initial proton PDFs; $x_{1,2}$ represent the longitudinal fractions of the partons involved in the hard subprocess; $d\hat{\sigma}_{r,s}\left(\hat{s}, \mu_F\right)$ is the partonic cross section for the production of jets and $\hat{s} \equiv x_1 x_2 s$ is the squared center-of-mass energy of the hard subprocess (see Fig. 1). The BFKL dynamics enters in the cross-section for the partonic hard subprocess $d\hat{\sigma}_{r,s}$ in the form of two forward gluon Green functions φ to be described in a while.

Using the definition of the jet vertex in the leading order approximation [41], we can present the cross section for the process as

$$\frac{d\sigma^{3-\mathrm{jet}}}{dk_A\, dY_A\, d\theta_A\, dk_B\, dY_B\, d\theta_B\, dk_J\, dy_J d\theta_J} = \frac{8\pi^3\, C_F\, \bar{\alpha}_s^3}{N_c^3}\, \frac{x_{J_A}\, x_{J_B}}{k_A\, k_B\, k_J} \int d^2\vec{p}_A \int d^2\vec{p}_B\, \delta^{(2)}\left(\vec{p}_A + \vec{k}_J - \vec{p}_B\right) \times \left(\frac{N_c}{C_F} f_g(x_{J_A}, \mu_F) + \sum_{r=q,\bar{q}} f_r(x_{J_A}, \mu_F)\right) \times \left(\frac{N_c}{C_F} f_g(x_{J_B}, \mu_F) + \sum_{s=q,\bar{q}} f_s(x_{J_B}, \mu_F)\right) \times \varphi\left(\vec{k}_A, \vec{p}_A, Y_A - y_J\right) \varphi\left(\vec{p}_B, \vec{k}_B, y_J - Y_B\right), \quad (4)$$

where N_c is the number of colors in QCD and C_F is the Casimir operator, $C_F = (N_c^2 - 1)/(2N_c)$. In order to lie within multi-Regge kinematics, we have considered the ordering in the rapidity of the produced particles $Y_A > y_J > Y_B$, while k_J^2 is always above the experimental resolution scale. $x_{J_{A,B}}$ are the longitudinal momentum fractions of the two external jets, linked to the respective rapidities $Y_{A,B}$ by the relation $x_{A,B} = k_{A,B}\, e^{\pm Y_{A,B}}/\sqrt{s}$. φ are BFKL gluon Green functions normalized to $\varphi\left(\vec{p}, \vec{q}, 0\right) = \delta^{(2)}\left(\vec{p} - \vec{q}\right)$ and $\bar{\alpha}_s$ is defined in terms of the strong coupling as $\bar{\alpha}_s = N_c/\pi\, \alpha_s\left(\mu_R\right)$.

Building up on the work in Refs. [36, 37], we study observables for which the BFKL approach will be distinct from other formalisms and also rather insensitive to possible higher order corrections. We focus on new quantities whose associated distributions are different from the ones which characterize the Mueller-Navelet case, though still related to the azimuthal-angle correlations by projecting the differential cross section on the two relative azimuthal angles between each external jet and the central one $\Delta\theta_{\widehat{AJ}} = \theta_A - \theta_J - \pi$ and $\Delta\theta_{\widehat{JB}} = \theta_J - \theta_B - \pi$ (see Fig. 2). Taking into account the factors coming from the jet vertices, it is possible to rewrite the projection of the differential cross section on the azimuthal angle differences (Eq. (7) in Ref. [36]) in the

form

$$\int_0^{2\pi} d\theta_A \int_0^{2\pi} d\theta_B \int_0^{2\pi} d\theta_J \cos\left(M\Delta\theta_{\widehat{AJ}}\right) \cos\left(N\Delta\theta_{\widehat{JB}}\right) \tag{5}$$

$$\frac{d\sigma^{3-\mathrm{jet}}}{dk_A\, dY_A\, d\theta_A\, dk_B\, dY_B\, d\theta_B\, dk_J\, dy_J d\theta_J} =$$

$$\frac{8\pi^4\, C_F\, \bar{\alpha}_s^3}{N_C^3}\, \frac{x_{J_A}\, x_{J_B}}{k_A\, k_B} \left(\frac{N_C}{C_F} f_g(x_{J_A}, \mu_F) \,+\, \sum_{r=q,\bar{q}} f_r(x_{J_A}, \mu_F)\right)$$

$$\times \left(\frac{N_C}{C_F} f_g(x_{J_B}, \mu_F) + \sum_{s=q,\bar{q}} f_s(x_{J_B}, \mu_F)\right) \sum_{L=0}^{N} \binom{N}{L} \left(k_J^2\right)^{\frac{L-1}{2}}$$

$$\times \int_0^\infty dp^2 \left(p^2\right)^{\frac{N-L}{2}} \int_0^{2\pi} d\theta \frac{(-1)^{M+N} \cos\left(M\theta\right) \cos\left((N-L)\theta\right)}{\sqrt{\left(p^2 + k_J^2 + 2pk_J \cos\theta\right)^N}}$$

$$\times\, \varphi_M^{(LLA,NLLA)}\left(k_A^2, p^2, Y_A - y_J\right) \varphi_N^{(LLA,NLLA)}\left(p^2 + k_J^2 + 2pk_J\cos\theta, k_B^2, y_J - Y_B\right).$$

In this expression the gluon Green function φ is either at LLA ($\varphi^{(LLA)}$) or at NLLA ($\varphi^{(NLLA)}$) accuracy. In particular, at LLA we have

$$\varphi_n^{(LLA)}\left(k^2, q^2, y\right) \;=\; 2\int_0^\infty d\nu \cos\left(\nu \ln\frac{k^2}{q^2}\right) \frac{e^{\bar{\alpha}_s \chi_{|n|}(\nu) y}}{\pi\sqrt{k^2 q^2}}, \tag{6}$$

while the LLA BFKL kernel $\chi_n\left(\nu\right)$ reads

$$\chi_n\left(\nu\right) \;=\; 2\,\psi(1) - \psi\left(\frac{1+n}{2} + i\nu\right) - \psi\left(\frac{1+n}{2} - i\nu\right) \tag{7}$$

and ψ is the logarithmic derivative of Euler's gamma function.

At NLLA we have

$$\varphi_n^{(NLLA)}\left(k^2, q^2, y\right) = 2\int_0^\infty d\nu \cos\left(\nu \ln\frac{k^2}{q^2}\right) \frac{e^{\bar{\alpha}_s\left(\chi_{|n|}(\nu) + \bar{\alpha}_s \chi_{|n|}^{(1)}(\nu)\right) Y}}{\pi\sqrt{k^2 q^2}}\,, \tag{8}$$

where the NLLA contribution $\chi_{|n|}^{(1)}(\nu)$, calculated in [48] (see also [49]), can be presented in the form

$$\chi_n^{(1)}(\nu) = -\frac{\beta_0}{8\, N_c}\left(\chi_n^2(\nu) - \frac{10}{3}\chi_n(\nu) - i\chi_n'(\nu)\right) + \bar{\chi}_n(\nu)\,, \tag{9}$$

with

$$-\,4\bar{\chi}_n(\nu) \;=\; \frac{\pi^2 - 4}{3}\chi_n(\nu) - 6\zeta(3) - \chi_n''(\nu) + \,2\,\phi_n(\nu) + \,2\,\phi_n(-\nu)$$

$$+\frac{\pi^2 \sinh(\pi\nu)}{2\,\nu\,\cosh^2(\pi\nu)} \left(\left(3 + \left(1 + \frac{n_f}{N_c^3}\right)\frac{11 + 12\nu^2}{16(1+\nu^2)}\right)\delta_{n0} - \left(1 + \frac{n_f}{N_c^3}\right)\frac{(1+4\nu^2)\delta_{n2}}{32(1+\nu^2)}\right), \tag{10}$$

and

$$\phi_n(\nu) = \sum_{k=0}^{\infty} \frac{(-1)^{k+1}}{k+(n+1)/2+i\nu} \left[\psi'(k+n+1) - \psi'(k+1) \right.$$
$$\left. +(-1)^{k+1}(\beta'(k+n+1)+\beta'(k+1)) - \frac{(\psi(k+n+1)-\psi(k+1))}{k+(n+1)/2+i\nu}\right], \quad (11)$$

whereas $4\beta'(z) = \psi'\left((z+1)/2\right) - \psi'\left(z/2\right)$.

In order to make an appropriate choice of the renormalization scale μ_R, we used the Brodsky-Lepage-Mackenzie (BLM) prescription [50] which is proven a very successful choice for fitting the data in Mueller-Navelet studies [31, 32]. It consists of using the MOM scheme and choosing the scale μ_R such that the β_0-dependence of a given observable vanishes. Applying the BLM prescription leads to the modification of the exponent in Eq. (8) in the following way:

$$\bar{\alpha}_s \left(\chi_{|n|}(\nu) + \bar{\alpha}_s \chi^{(1)}_{|n|}(\nu)\right) Y \;\rightarrow\; \bar{\alpha}_s \left(\chi_{|n|}(\nu)\left(1+\frac{\alpha_s}{\pi}T\right) + \bar{\alpha}_s \chi^{(1)}_{|n|}(\nu)\right) Y\,, \quad (12)$$

where

$$\begin{aligned} T &= T^{\beta} + T^{\,\mathrm{conf}}\,, \\ T^{\beta} &= -\frac{\beta_0}{2}\left(1+\frac{2}{3}I\right)\,, \\ T^{conf} &= \frac{C_A}{8}\left[\frac{17}{2}I + \frac{3}{2}\left(I-1\right)\xi + \left(1-\frac{1}{3}I\right)\xi^2 - \frac{1}{6}\xi^3\right]\,. \end{aligned}$$

Here $I = -2\int_0^1 dx \frac{\ln(x)}{x^2-x+1} \simeq 2.3439$ and ξ is a gauge parameter, fixed at zero.

Following this procedure, the renormalization scale μ_R is fixed at the value

$$(\mu_R^{\mathrm{BLM}})^2 = k_A k_B \;\exp\left[\frac{1+4I}{3} + \frac{1}{2}\chi_n\left(\nu\right)\right]\,. \quad (13)$$

In our numerical analysis we consider two cases. In one, we set $\mu_R = \mu_R^{\mathrm{BLM}}$ only in the exponential factor of the gluon Green function φ_n, while we let the argument of the $\bar{\alpha}_s^3$ in Eq. 5 to be at the 'natural' scale $\sqrt{k_A k_B}$, that is, $\bar{\alpha}_s^3(\sqrt{k_A k_B})$. In the second case, we fix $\mu_R = \mu_R^{\mathrm{BLM}}$ everywhere in Eq. 5. These two cases lead in general to two different but similar values for our NLLA predictions and wherever we present plots we fill the space in between so that we end up having a band instead of a single curve for the NLLA observables. The band represents the uncertainty that comes into play after using the BLM prescription since there is no unambiguous way to apply it.

The experimental observables we initially proposed are based on the partonic-level average values (with M, N being positive integers)

$$\begin{aligned} \mathcal{C}_{MN} &= \langle \cos\left(M\left(\theta_A - \theta_J - \pi\right)\right) \cos\left(N\left(\theta_J - \theta_B - \pi\right)\right) \rangle \\ &= \frac{\int_0^{2\pi} d\theta_A d\theta_B d\theta_J \cos\left(M\left(\theta_A - \theta_J - \pi\right)\right) \cos\left(N\left(\theta_J - \theta_B - \pi\right)\right) d\sigma^{3-\text{jet}}}{\int_0^{2\pi} d\theta_A d\theta_B d\theta_J d\sigma^{3-\text{jet}}}, \end{aligned} \tag{14}$$

whereas, in order to provide testable predictions for the current and future experimental data, we introduce the hadronic-level values C_{MN} after integrating $\mathcal{C}_{M,N}$ over the momenta of the tagged jets, as we will see in the following sections.

From a more theoretical perspective, it is important to have as good as possible perturbative stability in our predictions (see [18] for a related discussion). This can be achieved by removing the contribution stemming from the zero conformal spin, which corresponds to the index $n = 0$ in Eqs. (6) and (8). We, therefore, introduce the ratios

$$R_{PQ}^{MN} = \frac{C_{MN}}{C_{PQ}} \tag{15}$$

which are free from any $n = 0$ dependence, as long as $M, N, P, Q > 0$. The postulate that Eq. 15 generally describes observables with good perturbative stability is under scrutiny in Sections 3, 4 and 5 where we compare LLA and NLLA results.

Before we proceed to our numerical results in the next sections, we should give a few details with regard to our numerical computations. From all the possible ratios, we have chosen to study the following three: R_{22}^{12}, R_{33}^{12} and R_{33}^{22}. These are enough to have an adequate view of how the generic R_{PQ}^{MN} behaves. We computed R_{22}^{12}, R_{33}^{12} and R_{33}^{22} in all cases almost exclusively in FORTRAN whereas MATHEMATICA was used mainly for cross-checks. The NLO MSTW 2008 PDF sets [51] were used and for the strong coupling α_s we chose a two-loop running coupling setup with $\alpha_s\left(M_Z\right) = 0.11707$ and five quark flavours. We made extensive use of the integration routine `Vegas` [52] as implemented in the `Cuba` library [53, 54]. Furthermore, we used the `Quadpack` library [55] and a slightly modified version of the `Psi` [56] routine.

3 R_{22}^{12}, R_{33}^{12} and R_{33}^{22} with the central jet fixed in rapidity

In this section, we will present results for three generalised ratios, R_{22}^{12}, R_{33}^{12} and R_{33}^{22}, assuming that the central jet is fixed in rapidity at $y_J = (Y_A + Y_B)/2$

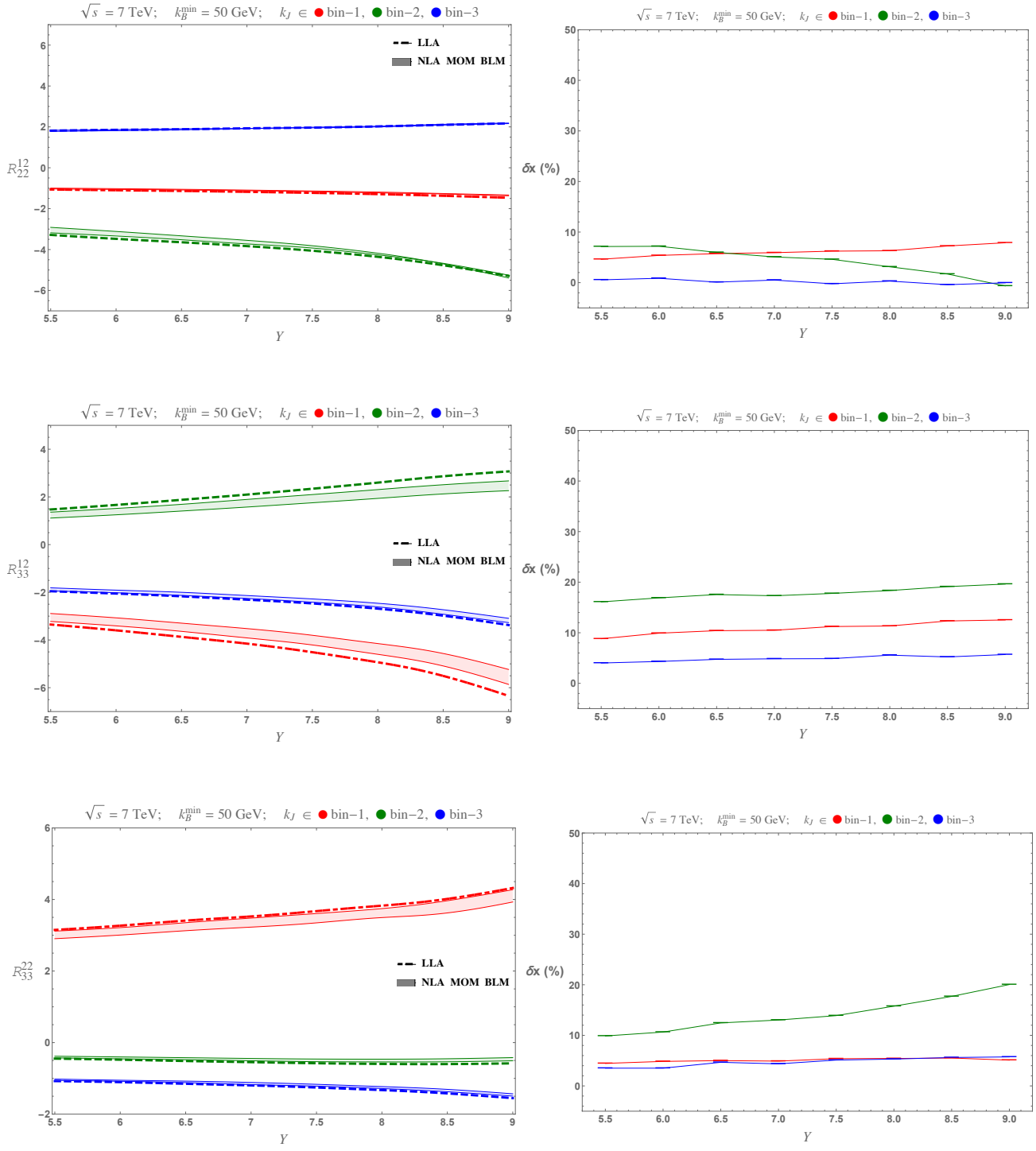

Figure 3: Y-dependence of the LLA and NLLA R_{22}^{12}, R_{33}^{12} and R_{33}^{22} at $\sqrt{s} = 7$ TeV with y_J fixed (left) and the relative NLLA to LLA corrections (right).

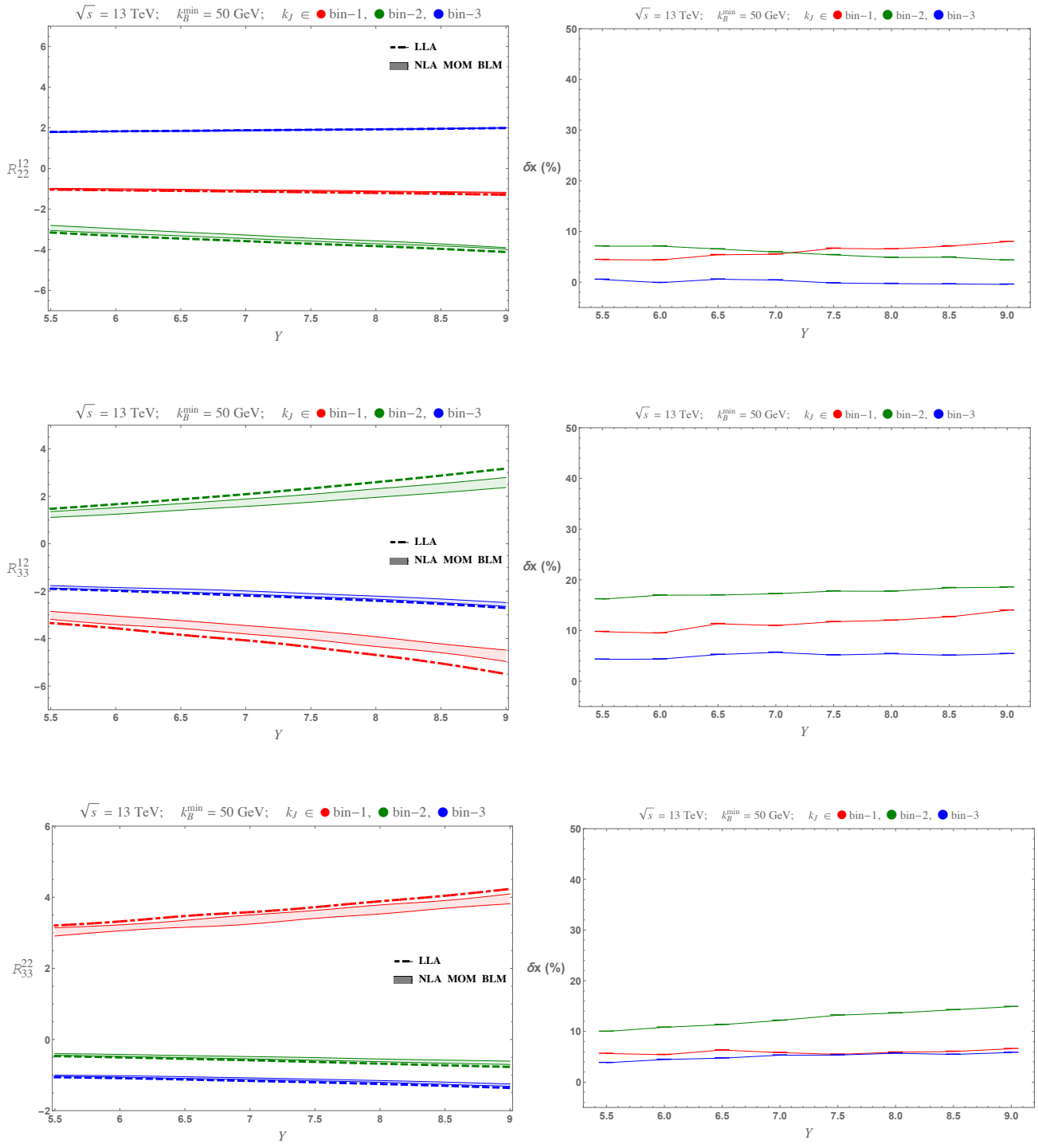

Figure 4: Y-dependence of the LLA and NLLA R_{22}^{12}, R_{33}^{12} and R_{33}^{22} at $\sqrt{s} = 13$ TeV with y_J fixed (left) and the relative NLLA to LLA corrections (right).

(see Fig. 2). In particular,

$$C_{MN} = \int_{Y_A^{\rm min}}^{Y_A^{\rm max}} dY_A \int_{Y_B^{\rm min}}^{Y_B^{\rm max}} dY_B \int_{k_A^{\rm min}}^{k_A^{\rm max}} dk_A \int_{k_B^{\rm min}}^{k_B^{\rm max}} dk_B \int_{k_J^{\rm min}}^{k_J^{\rm max}} dk_J \delta\left(Y_A - Y_B - Y\right) \mathcal{C}_{MN}, \tag{16}$$

where the forward jet rapidity is taken in the range delimited by $0 < Y_A < 4.7$, the backward jet rapidity in the range $-4.7 < Y_B < 0$, while their difference $Y \equiv Y_A - Y_B$ is kept fixed at definite values in the range $5.5 < Y < 9$.

We can now study the ratios $R_{PQ}^{MN}(Y)$ in Eq. (15) as functions of the rapidity difference Y between the most forward and the most backward jets for a set of characteristic values of M, N, P, Q and for two different center-of-mass energies: $\sqrt{s} = 7$ and $\sqrt{s} = 13$ TeV. Since we are integrating over k_A and k_B, we have the opportunity to impose either symmetric or asymmetric kinematic cuts, as it has been previously done in Mueller-Navelet studies. Here, and for the rest of the paper, we choose to study the asymmetric cut which presents certain advantages over the symmetric one (see Refs. [22, 34]). To be more precise, we set $k_A^{\rm min} = 35$ GeV, $k_B^{\rm min} = 50$ GeV, $k_A^{\rm max} = k_B^{\rm max} = 60$ GeV throughout the paper.

In order to be as close as possible to the characteristic rapidity ordering of the multi-Regge kinematics, we set the value of the central jet rapidity such that it is equidistant to Y_A and Y_B by imposing the condition $y_J = (Y_A + Y_B)/2$. Moreover, since the tagging of a central jet permits us to extract more exclusive information from our observables, we allow three possibilities for the transverse momentum k_J, that is, $20\,{\rm GeV} < k_J < 35\,{\rm GeV}$ (bin-1), $35\,{\rm GeV} < k_J < 60\,{\rm GeV}$ (bin-2) and $60\,{\rm GeV} < k_J < 120\,{\rm GeV}$ (bin-3). Keeping in mind that the forward/backward jets have transverse momenta in the range $[35\,{\rm GeV}, 60\,{\rm GeV}]$, restricting the value of k_J within these three bins allows us to see how the ratio $R_{PQ}^{MN}(Y)$ changes its behaviour depending on the relative size of the central jet momentum when compared to the forward/backward ones. Throughout the paper, we will keep the same setup regarding bin-1, bin-2 and bin-3 which roughly correspond to the cases of k_J being 'smaller' than, 'similar' to and 'larger' than k_A, k_B, respectively.

Finally, apart from the functional dependence of the ratios on Y we will also show the relative corrections when we go from LLA to NLLA. To be more precise, we define

$$\delta x(\%) = \left({\rm res}^{\rm (LLA)} - \frac{{\rm res}^{\rm (BLM-1)} + {\rm res}^{\rm (BLM-2)}}{2} \right) \frac{1}{{\rm res}^{\rm (LLA)}}\,. \tag{17}$$

${\rm res}^{\rm (BLM-1)}$ is the BLM NLLA result for $\mu_R = \mu_R^{\rm BLM}$ only in the gluon Green function while the cubed term of the strong coupling in Eq. 5 actually reads

$\bar{\alpha}_s^3 = \bar{\alpha}_s^3(\sqrt{k_A k_B})$). res$^{(\mathrm{BLM}-2)}$ is the BLM NLLA result for $\mu_R = \mu_R^{\mathrm{BLM}}$ everywhere in Eq. 5, therefore, $\bar{\alpha}_s^3 = \bar{\alpha}_s^3(\mu_R^{\mathrm{BLM}})$, as was previously discussed in Section 2.

In the following, we present our results for R_{22}^{12}, R_{33}^{12} and R_{33}^{22}, with $y_J = (Y_A + Y_B)/2$, collectively in Fig. 3 ($\sqrt{s} = 7$ TeV) and Fig. 4 ($\sqrt{s} = 13$ TeV), In the left column we are showing plots for $R_{PQ}^{MN}(Y)$ whereas to the right we are showing the corresponding $\delta x(\%)$ between LLA and NLLA corrections. The LLA results are represented with dashed lines whereas the NLLA ones with a continuous band. The boundaries of the band are the two different curves we obtain by the two different approaches in applying the BLM prescription. Since there is no definite way to choose one in favour of the other, we allow for any possible value in between and hence we end up with a band. In many cases, as we will see in the following, the two boundaries are so close that the band almost degenerates into a single curve. The red curve (band) corresponds to k_J bounded in bin-1, the green curve (band) to k_J bounded in bin-2 and finally the blue curve (band) to k_J bounded in bin-3. For the $\delta x(\%)$ plots we only have three curves, one for each of the three different bins of k_J.

A first observation from inspecting Figs. 3 and 4 is that the dependence of the different observables on the rapidity difference between k_A and k_B is rather smooth. R_{22}^{12} (top row in Figs. 3 and 4) at $\sqrt{s} = 7$ TeV and for k_J in bin-1 and bin-3 exhibits an almost linear behaviour with Y both at LLA and NLLA, whereas at $\sqrt{s} = 13$ TeV the linear behaviour is extended also for k_J in bin-2. The difference between the NLLA BLM-1 and BLM-2 values is small, to the point that the blue and the red bands collapse into a single line which in addition lies very close to the LLA results. When k_J is restricted in bin-2 (green curve/band), the uncertainty from applying the BLM prescription in two different ways seems to be larger. The relative NLLA corrections at both colliding energies are very modest ranging from close to 1% for k_J in bin-3 to less than 10% for k_J in the other two bins.

R_{33}^{12} (middle row in Figs. 3 and 4) compared to R_{22}^{12}, shows a larger difference between BLM-1 and BLM-2 values for k_J in bin-1 and bin-2. The 'green' corrections lower the LLA estimate whereas the 'red' ones make the corresponding LLA estimate less negative. The corrections are generally below 20%, in particular, 'blue' $\sim 5\%$, 'red' $\sim 10\%$ and 'green' $\sim 20\%$.

Finally, R_{33}^{22} (bottom row in Figs. 3 and 4) also shows a larger difference between BLM-1 and BLM-2 values for k_J in bin-1 and less so for k_J in bin-2. Here, the 'red' corrections lower the LLA estimate whereas the 'green' ones make the corresponding LLA estimate less negative. The corrections are smaller than the ones for R_{33}^{12} and somehow larger than the corrections for R_{22}^{12}, specifically, 'blue' $\sim 5\%$, 'red' $\sim 5\%$ and 'green' $\sim 15\%$. Noticeably, while for R_{22}^{12} and R_{33}^{12} the corrections are very similar at $\sqrt{s} = 7$ and $\sqrt{s} = 13$ TeV, the 'green' R_{33}^{22} receives larger corrections at $\sqrt{s} = 7$ TeV.

One important conclusion we would like to draw after comparing Figs. 3 and 4 is that, in general, for most of the observables there are no striking changes when we increase the colliding energy from 7 to 13 TeV. This indicates that a sort of asymptotic regime has been approached for the kinematical configurations included in our analysis. It also tells us that our observables are really as insensitive as possible to effects which have their origin outside the BFKL dynamics and which normally cannot be isolated (*e.g.* influence from the PDFs) with a possible exclusion at the higher end of the plots, when $Y \sim 8.5 - 9$. There, some of the observables and by that we mean the 'red', 'green' or 'blue' cases of R_{22}^{12}, R_{33}^{12} and R_{33}^{22}, exhibit a more curved rather than linear behaviour with Y at $\sqrt{s} = 7$ TeV.

4 R_{22}^{12}, R_{33}^{12} and R_{33}^{22} after integration over a central jet rapidity bin

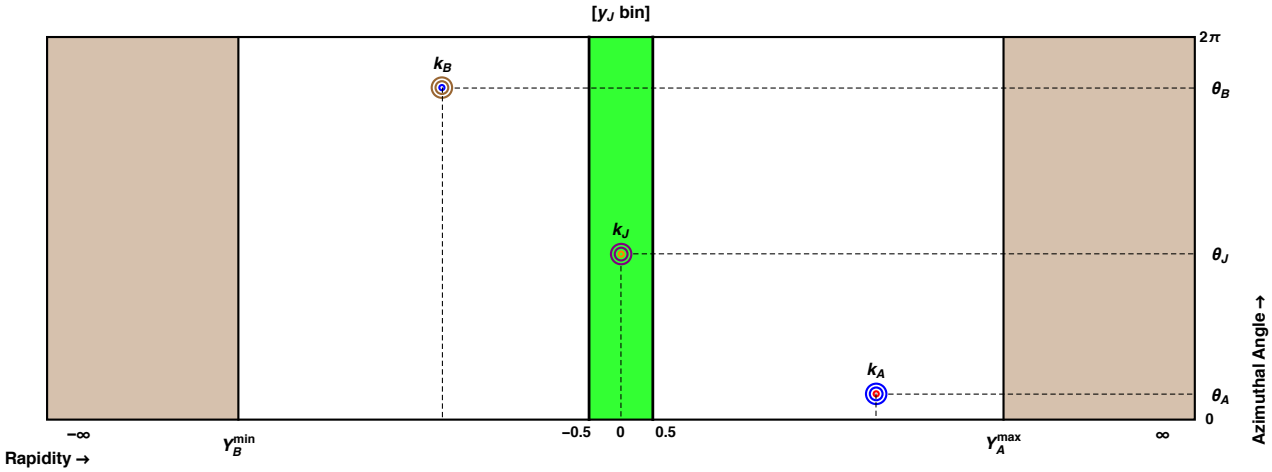

Figure 5: A primitive lego plot depicting a three-jet event similar to Fig. 5. Here, however, the central jet can take any value in the rapidity range $-0.5 < y_J < 0.5$.

In this section, everything is kept the same as in Section 3 with the exemption of the allowed values for y_J (see Fig. 5). While in the previous section $y_J = (Y_A + Y_B)/2$, here y_J is not anymore dependent on the rapidity difference between the outermost jets, Y, and is allowed to take values in a rapidity bin around $y_J = 0$. In particular, $-0.5 < y_J < 0.5$, which in turn means that an additional integration over y_J needs to be considered in

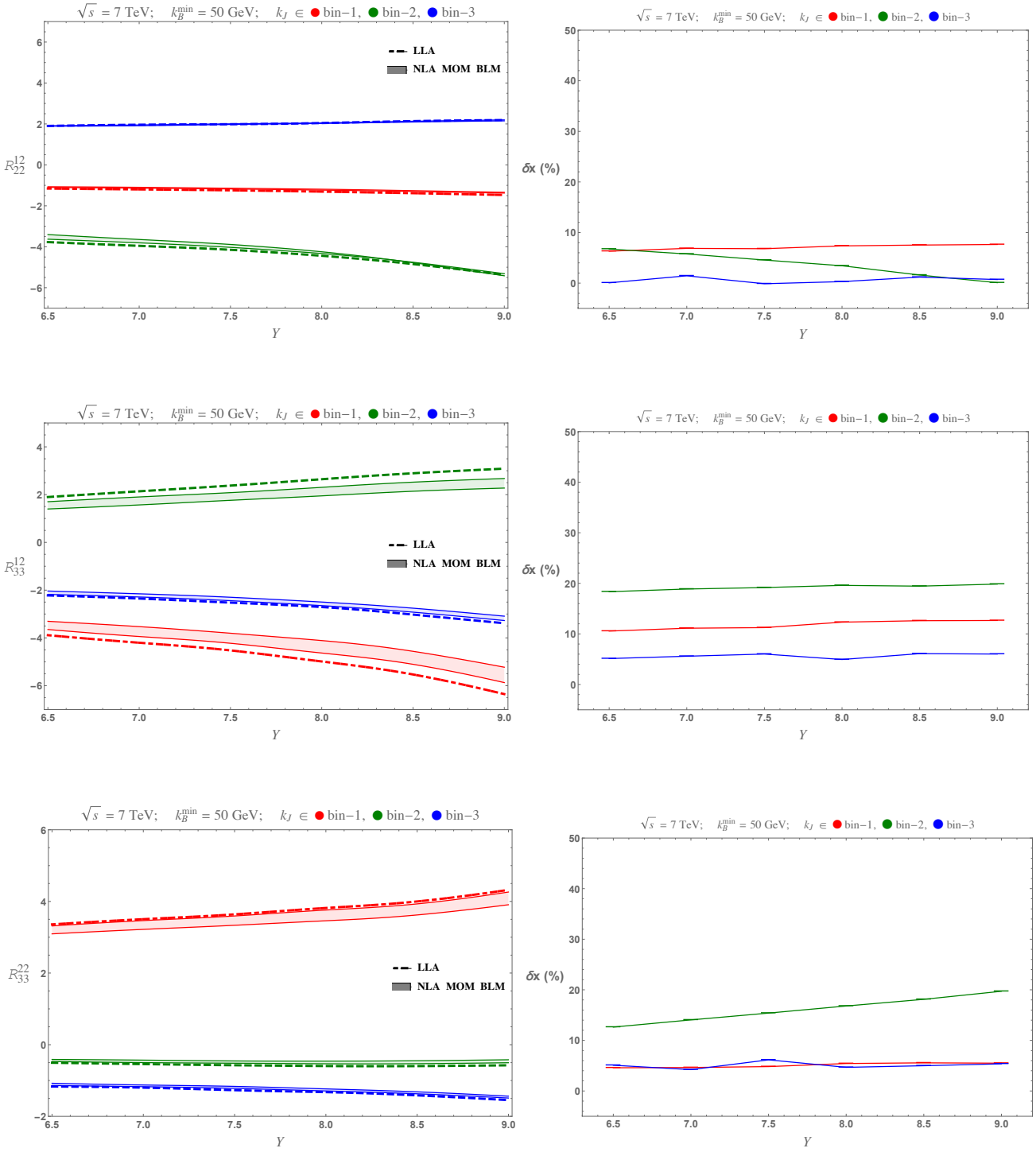

Figure 6: Y-dependence of the LLA and NLLA R_{22}^{12}, R_{33}^{12} and R_{33}^{22} at $\sqrt{s} = 7$ TeV with y_J integrated over a central rapidity bin (left) and the relative NLLA to LLA corrections (right).

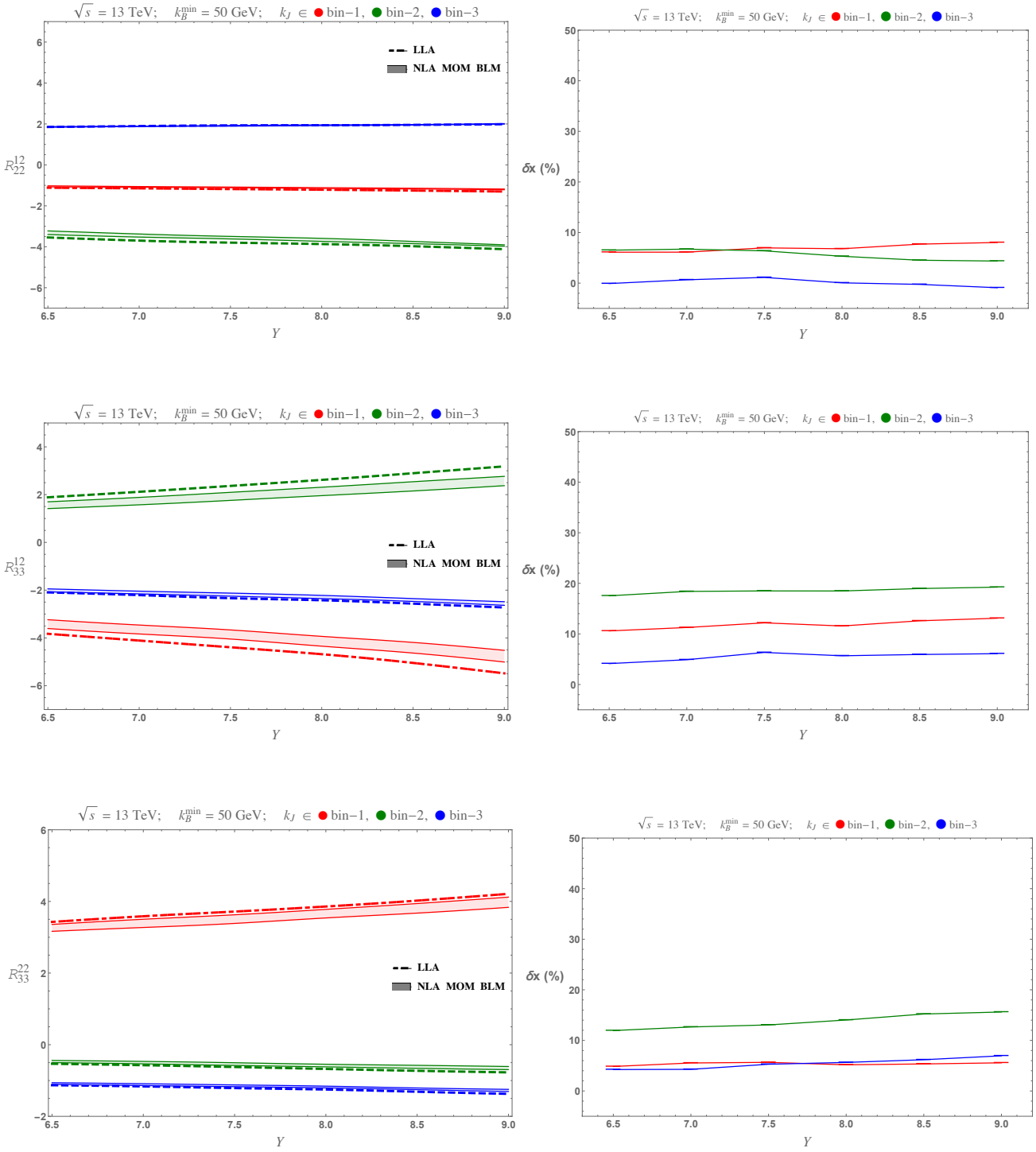

Figure 7: Y-dependence of the LLA and NLLA R_{22}^{12}, R_{33}^{12} and R_{33}^{22} at $\sqrt{s} = 13$ TeV with y_J integrated over a central rapidity bin (left) and the relative NLLA to LLA corrections (right).

Eq. 16 with $y_J^{\min} = -0.5$ and $y_J^{\max} = 0.5$:

$$C_{MN}^{\text{integ}} = \int_{y_J^{\min}}^{y_J^{\max}} dy_J \int_{Y_A^{\min}}^{Y_A^{\max}} dY_A \int_{Y_B^{\min}}^{Y_B^{\max}} dY_B \int_{k_A^{\min}}^{k_A^{\max}} dk_A \int_{k_B^{\min}}^{k_B^{\max}} dk_B \int_{k_J^{\min}}^{k_J^{\max}} dk_J \delta\left(Y_A - Y_B - Y\right) \mathcal{C}_{MN}, \tag{18}$$

With a slight abuse of notation, we will keep denoting our observables R_{PQ}^{MN}:

$$R_{PQ}^{MN} = \frac{C_{MN}^{\text{integ}}}{C_{PQ}^{\text{integ}}}. \tag{19}$$

Therefore, in Figs. 6 and 7 we still have R_{22}^{12}, R_{33}^{12} and R_{33}^{22} although here they do contain the extra integration over y_J.

We notice immediately that Fig. 3 is very similar to the integrated over y_J observables in Fig. 6 and the same holds for Figs. 4 and 7. Therefore, we will not discuss here the individual behaviours of R_{22}^{12}, R_{33}^{12} and R_{33}^{22} with Y, neither the $\delta x(\%)$ corrections, since this would only mean to repeat the discussion of the previous section. We would like only to note that the striking similarity between Fig. 3 and Fig. 6 and between Fig. 4 and Fig. 7 was to be expected if we remember that the partonic-level quantities $\mathcal{R}_{PQ}^{MN}$ do not change noticeably if we vary the position in rapidity of the central jet, as long as the position remains "sufficiently" central (see Ref. [36]). This property is very important and we will discuss it more in the next section. Here, we should stress that the observables as presented in this section can be readily compared to experimental data.

5 R_{22}^{12}, R_{33}^{12} and R_{33}^{22} after integration over a forward, backward and central rapidity bin

In this section, we present an alternative kinematical configuration (see Fig. 8) for the generalised ratios R_{PQ}^{MN}. We do this for two reasons. Firstly, to offer a different setup for which the comparison between theoretical predictions and experimental data might be easier, compared to the previous section. Secondly, to demonstrate that the generalised ratios do capture the Bethe-Salpeter characteristics of the BFKL radiation. The latter needs a detailed explanation.

Let us assume that we have a gluonic ladder exchanged in the t-channel between a forward jet (at rapidity Y_A) and a backward jet (at rapidity Y_B)

accounting for minijet activity between the two jets. By gluonic ladder here we mean the gluon Green function $\varphi\left(\vec{p}_A, \vec{p}_B, Y_A - Y_B\right)$, where $\vec{p}_A$ and $\vec{p}_B$ are the reggeized momenta connected to the forward and backward jet vertex respectively. It is known that the following relation holds for the gluon Green function:

$$\varphi\left(\vec{p}_A, \vec{p}_B, Y_A - Y_B\right) \;=\; \int d^2\vec{k}\, \varphi\left(\vec{p}_A, \vec{k}, Y_A - y\right) \varphi\left(\vec{k}, \vec{p}_B, y - Y_B\right). \quad (20)$$

In other words, one may 'cut' the gluonic ladder at any rapidity y between Y_A and Y_B and then integrate over the reggeized momentum $\vec{k}$ that flows in the t-channel, to recover the initial ladder. Which value of y one chooses to 'cut' the ladder at is irrelevant. Therefore, observables directly connected to a realisation of the r.h.s of Eq. 20 should display this y-independence.

In our study actually, we have a very similar picture as the one described in the r.h.s of Eq. 20. The additional element is that we do not only 'cut' the gluonic ladder but we also 'insert' a jet vertex for the central jet. This means that the y-independence we discussed above should be present in one form or another. To be precise, we do see the y-independence behaviour but now we have to consider the additional constraint that y cannot take any extreme values, that is, it cannot be close to Y_A or Y_B. For a more detailed discussion of Eq. 20, we refer the reader to Appendix A, here we will proceed to present our numerical results.

The kinematic setup now is different than in the previous sections. We allow Y_A and Y_B to take values such that $(Y_A^{\min} = 3) < Y_A < (Y_A^{\max} = 4.7)$ and $(Y_B^{\min} = -4.7) < Y_B < (Y_B^{\max} = -3)$. Moreover, we allow for the rapidity of the central jet to take values in five distinct rapidity bins of unit width, that is, $y_i - 0.5 < y_J < y_i + 0.5$, with $y_i = \{-1, -0.5, 0, 0.5, 1\}$ and we define the coefficients $C_{MN}^{\text{integ}}(y_i)$ as function of y_i:

$$C_{MN}^{\text{integ}}(y_i) = \int_{y_i-0.5}^{y_i+0.5} dy_J \int_{Y_A^{\min}}^{Y_A^{\max}} dY_A \int_{Y_B^{\min}}^{Y_B^{\max}} dY_B \int_{k_A^{\min}}^{k_A^{\max}} dk_A \int_{k_B^{\min}}^{k_B^{\max}} dk_B \int_{k_J^{\min}}^{k_J^{\max}} dk_J\; \mathcal{C}_{MN}. \quad (21)$$

Again, keeping our notation with regard to the ratios uniform, we continue denoting our observables by R_{PQ}^{MN} but now the ratios are functions of y_i instead of Y:

$$R_{PQ}^{MN}(y_i) \;=\; \frac{C_{MN}^{\text{integ}}(y_i)}{C_{PQ}^{\text{integ}}(y_i)}\,. \quad (22)$$

We present our results in Figs. 9 and 10. We see that indeed, the y_i-dependence of the three ratios is very weak. Moreover, the similarity between the $\sqrt{s} = 7$ TeV and $\sqrt{s} = 13$ TeV plots is more striking that in the previous sections. The relative NLLA to LLA corrections seem to be slightly

larger here than in the previous sections. We would like to stress once more that the results in this section are readily comparable to the experimental data once the same cuts are applied in the experimental analysis.

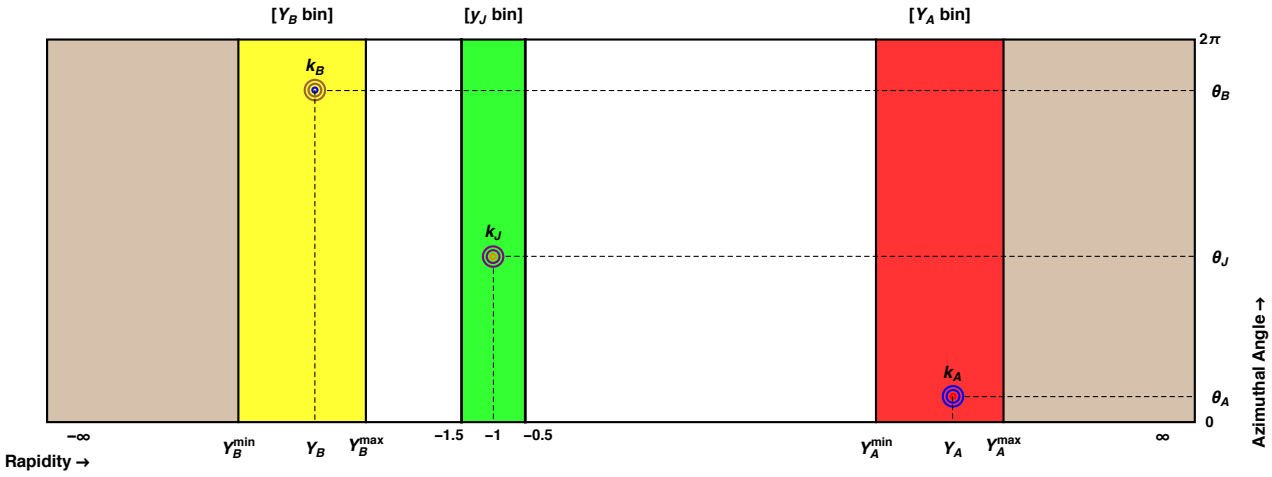

Figure 8: A primitive lego plot depicting a three-jet event similar to Fig. 5. Here, however, the rapidity of the central jet can take any value in the distinct ranges $y_i - 0.5 < y_J < y_i + 0.5$, where y_i is the central value of the rapidity bin with $y_i = \{-1, -0.5, 0, 0.5, 1\}$. In this figure, $y_i = -1$. Moreover, $Y = Y_A - Y_B$ is not anymore fixed. Instead, the forward jet has a rapidity restricted in the red bin whereas the backward jet in the yellow bin.

6 Summary & Outlook

We have presented a first complete phenomenological study beyond the LLA of inclusive three-jet production at the LHC within the BFKL framework, focussing on azimuthal-angle dependent observables. We considered two colliding energies, $\sqrt{s} = 7, 13$ TeV and an asymmetric kinematic cut with respect to the transverse momentum of the forward (k_A) and backward (k_B) jets. In addition, we have chosen to consider an extra condition regarding the value of the transverse momentum k_J of the central jet, dividing the allowed region for k_J into three sub-regions: k_J smaller than $k_{A,B}$, k_J similar to $k_{A,B}$ and k_J larger than $k_{A,B}$.

For a proper study at full NLLA, one needs to consider the NLO jet vertices and the NLLA gluon Green functions. We have argued that we expect the latter to be of higher relevance and we proceed to calculate them using the BLM prescription which has been successful in previous phenomenological analyses. We have shown how our observables R_{22}^{12}, R_{33}^{12}

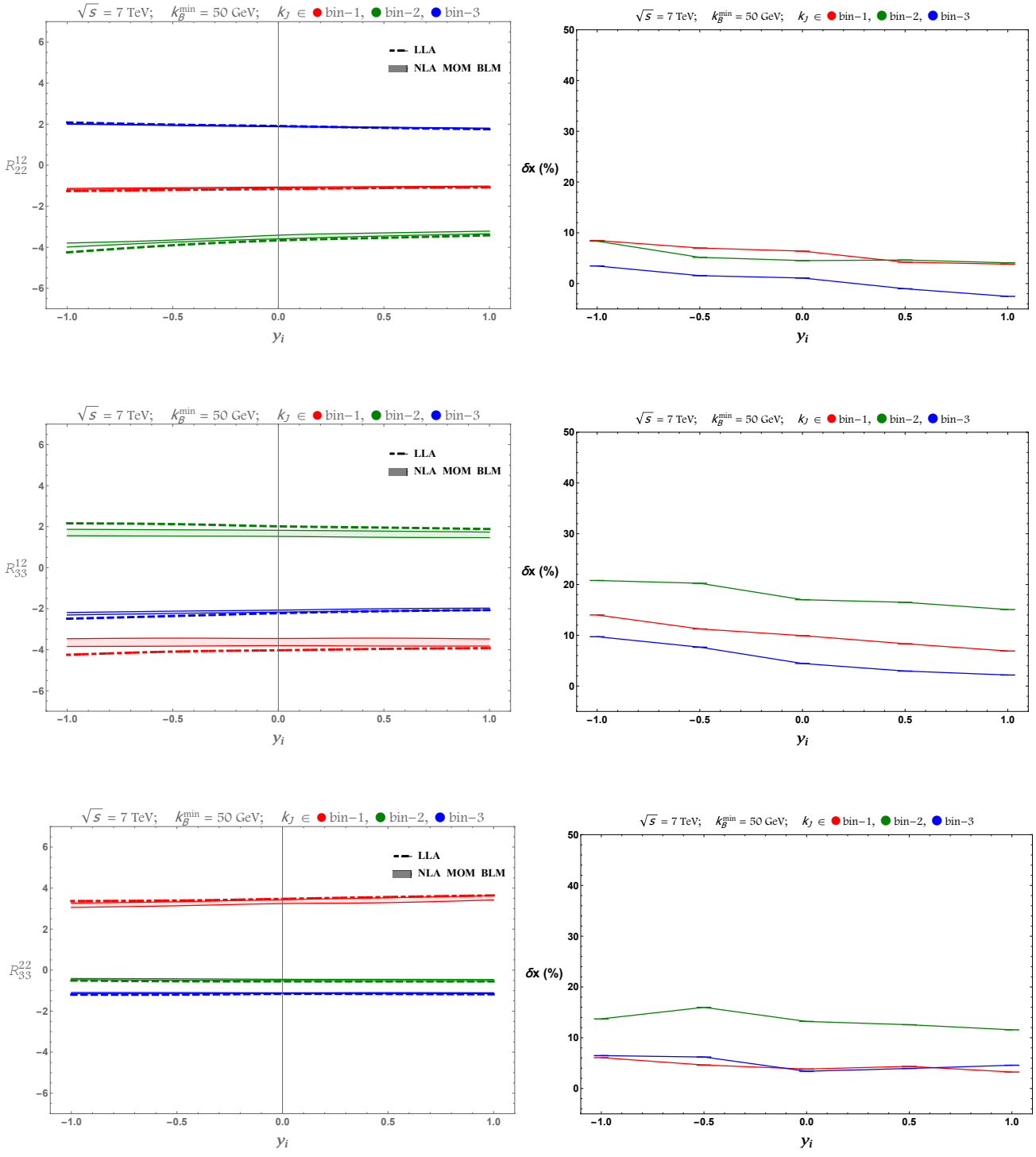

Figure 9: y_i-dependence of the LLA and NLLA R_{22}^{12}, R_{33}^{12} and R_{33}^{22} at $\sqrt{s} = 7$ TeV (left) and the relative NLLA to LLA corrections (right).

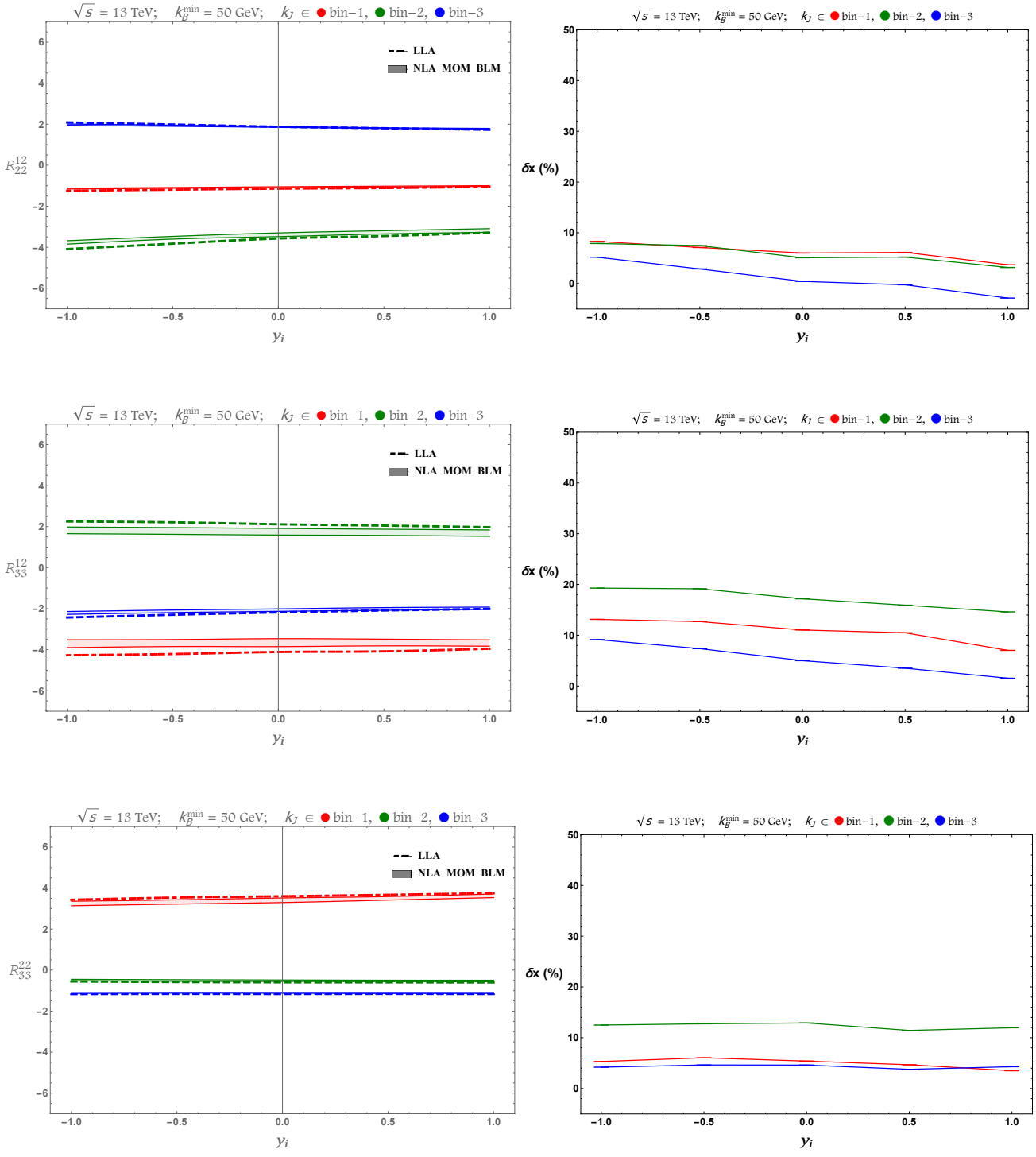

Figure 10: y_i-dependence of the LLA and NLLA R_{22}^{12}, R_{33}^{12} and R_{33}^{22} at $\sqrt{s} = 13$ TeV (left) and the relative NLLA to LLA corrections (right).

and R_{33}^{22} change when we vary the rapidity difference Y between k_A and k_B from 5.5 to 9 units for a fixed y_J and from 6.5 to 9 units for $-0.5 < y_J < 0.5$. We have presented both the LLA and NLLA results along with plots that show the relative size of the NLLA corrections compared to the LLA ones. We have also presented an alternative kinematical setup where we allow for Y_A and Y_B to take values such that $3 < Y_A < 4.7$ and $-4.7 < Y_B < -3$, while the rapidity of the central jet takes values in five distinct rapidity bins of unit width, that is, $y_i - 0.5 < y_J < y_i + 0.5$, with $y_i = \{-1, -0.5, 0, 0.5, 1\}$. In this alternative setup, we presented our results for R_{12}^{22}, R_{12}^{33} and R_{22}^{33} as functions of y_i.

The general conclusion is that the NLLA corrections are moderate and our proposed observables exhibit a good perturbative stability. Furthermore, we see that for a wide range of rapidities, the changes we notice when going from 7 TeV to 13 TeV are small which makes us confident that these generalised ratios pinpoint the crucial characteristics of the BFKL dynamics regarding the azimuthal behavior of the hard jets in inclusive three-jet production. It will be very interesting to compare with possible predictions for these observables from fixed order analyses as well as from the BFKL inspired Monte Carlo `BFKLex` [57, 58, 59, 60, 61, 62, 63, 64]. Predictions from general-purpose Monte Carlos tools should also be welcome. It would be extremely interesting to pursue an experimental analysis for these observables using LHC data.

Acknowledgements

GC acknowledges support from the MICINN, Spain, under contract FPA2013-44773-P. ASV acknowledges support from Spanish Government (MICINN (FPA2010-17747,FPA2012-32828)) and, together with FC and FGC, to the Spanish MINECO Centro de Excelencia Severo Ochoa Programme (SEV-2012-0249). DGG is supported with a fellowship of the international programme "La Caixa-Severo Ochoa". FGC thanks the Instituto de Física Teórica (IFT UAM-CSIC) in Madrid for warm hospitality.

A y_J independent integrated distributions

We show now how Eq. 20 is fulfilled in our normalisations. We introduce the notation $t = \ln k^2$ to write the gluon Green function in the form

$$\begin{aligned} \varphi\left(t_A, t_B, \theta_A, \theta_B, Y\right) &= \frac{e^{-\frac{t_A+t_B}{2}}}{\pi^2} \sum_{n=-\infty}^{\infty} e^{in(\theta_A-\theta_B)} \\ &\int_0^{\infty} d\nu \cos\left(\nu\left(t_A - t_B\right)\right) e^{\bar{\alpha}_s \chi_{|n|}(\nu) Y}. \end{aligned} \tag{23}$$

Making use of $dk = \frac{1}{2}e^{\frac{t}{2}}dt$ and $k\,dk\,d\theta = \frac{e^t}{2}d\theta$ we then want to show that

$$\begin{aligned}\varphi\left(t_A,t_B,\theta_A,\theta_B,Y\right) &= \int_0^{2\pi}d\theta\int_{-\infty}^{\infty}dt\,\frac{e^t}{2}\varphi\left(t_A,t,\theta_A,\theta,y\right)\varphi\left(t,t_B,\theta,\theta_B,Y-y\right)\\ &= \int_0^{2\pi}d\theta\int_{-\infty}^{\infty}dt\,\frac{e^t}{2}\frac{e^{-\frac{t_A+t}{2}}}{\pi^2}\sum_{m=-\infty}^{\infty}e^{im(\theta_A-\theta)}\int_0^{\infty}d\nu\cos\left(\nu\left(t_A-t\right)\right)e^{\bar{\alpha}_s\chi_{|m|}(\nu)y}\\ &\quad\frac{e^{-\frac{t+t_B}{2}}}{\pi^2}\sum_{n=-\infty}^{\infty}e^{in(\theta-\theta_B)}\int_0^{\infty}d\mu\cos\left(\mu\left(t-t_B\right)\right)e^{\bar{\alpha}_s\chi_{|n|}(\mu)(Y-y)}. \qquad (24)\end{aligned}$$

The integration over θ generates a δ_m^n contribution:

$$\begin{aligned}&\varphi\left(t_A,t_B,\theta_A,\theta_B,Y\right) =\\ &\quad\frac{e^{-\frac{t_A+t_B}{2}}}{\pi^3}\sum_{n=-\infty}^{\infty}e^{in(\theta_A-\theta_B)}\int_0^{\infty}d\nu\,e^{\bar{\alpha}_s\chi_{|n|}(\nu)y}\\ &\quad\int_0^{\infty}d\mu\,e^{\bar{\alpha}_s\chi_{|n|}(\mu)(Y-y)}\int_{-\infty}^{\infty}dt\cos\left(\nu\left(t_A-t\right)\right)\cos\left(\mu\left(t-t_B\right)\right). \qquad (25)\end{aligned}$$

It can be shown that

$$\begin{aligned}&\int_{-\infty}^{\infty}dt\cos\left(\nu\left(t_A-t\right)\right)\cos\left(\mu\left(t-t_B\right)\right) =\\ &\qquad\pi\Big(\cos\left(\nu t_A-\mu t_B\right)\delta(\nu-\mu)+\cos\left(\nu t_A+\mu t_B\right)\delta(\nu+\mu)\Big), \qquad (26)\end{aligned}$$

which can be used to write Eq. 25 as

$$\begin{aligned}&\varphi\left(t_A,t_B,\theta_A,\theta_B,Y\right) =\\ &\quad\frac{e^{-\frac{t_A+t_B}{2}}}{2\pi^2}\sum_{n=-\infty}^{\infty}e^{in(\theta_A-\theta_B)}\int_{-\infty}^{\infty}d\nu\int_0^{\infty}d\mu\,e^{\bar{\alpha}_s\chi_{|n|}(\mu)(Y-y)}e^{\bar{\alpha}_s\chi_{|n|}(\nu)y}\\ &\qquad\Big(\cos\left(\nu t_A-\mu t_B\right)\delta(\nu-\mu)+\cos\left(\nu t_A+\mu t_B\right)\delta(\nu+\mu)\Big), \qquad (27)\end{aligned}$$

and, finally,

$$\begin{aligned}&\varphi\left(t_A,t_B,\theta_A,\theta_B,Y\right) =\\ &\quad\frac{e^{-\frac{t_A+t_B}{2}}}{\pi^2}\sum_{n=-\infty}^{\infty}e^{in(\theta_A-\theta_B)}\int_0^{\infty}d\mu\,e^{\bar{\alpha}_s\chi_{|n|}(\mu)Y}\cos\left(\mu(t_A-t_B)\right), \qquad (28)\end{aligned}$$

which is the same as our initial representation for φ in Eq. 23. The relation in Eq. 24 is remarkable because it holds for any rapidity y.

References

[1] L. N. Lipatov, Sov. Phys. JETP **63** (1986) 904 [Zh. Eksp. Teor. Fiz. **90** (1986) 1536].

[2] I. I. Balitsky and L. N. Lipatov, Sov. J. Nucl. Phys. **28** (1978) 822 [Yad. Fiz. **28** (1978) 1597].

[3] E. A. Kuraev, L. N. Lipatov and V. S. Fadin, Sov. Phys. JETP **45** (1977) 199 [Zh. Eksp. Teor. Fiz. **72** (1977) 377].

[4] E. A. Kuraev, L. N. Lipatov and V. S. Fadin, Sov. Phys. JETP **44** (1976) 443 [Zh. Eksp. Teor. Fiz. **71** (1976) 840] [Erratum-ibid. **45** (1977) 199].

[5] L. N. Lipatov, Sov. J. Nucl. Phys. **23** (1976) 338 [Yad. Fiz. **23** (1976) 642].

[6] V. S. Fadin, E. A. Kuraev and L. N. Lipatov, Phys. Lett. B **60** (1975) 50.

[7] V. S. Fadin and L. N. Lipatov, Phys. Lett. B **429** (1998) 127 [hep-ph/9802290].

[8] M. Ciafaloni and G. Camici, Phys. Lett. B **430** (1998) 349 [hep-ph/9803389].

[9] A. H. Mueller and H. Navelet, Nucl. Phys. B **282** (1987) 727.

[10] D. Y. Ivanov and A. Papa, JHEP **1207**, 045 (2012) [arXiv:1205.6068 [hep-ph]].

[11] F. G. Celiberto, D. Y. Ivanov, B. Murdaca and A. Papa, Phys. Rev. D **94**, no. 3, 034013 (2016) doi:10.1103/PhysRevD.94.034013 [arXiv:1604.08013 [hep-ph]].

[12] V. Del Duca and C. R. Schmidt, Phys. Rev. D **49** (1994) 4510 [hep-ph/9311290].

[13] W. J. Stirling, Nucl. Phys. B **423** (1994) 56 [hep-ph/9401266].

[14] L. H. Orr and W. J. Stirling, Phys. Rev. D **56** (1997) 5875 [hep-ph/9706529].

[15] J. Kwiecinski, A. D. Martin, L. Motyka and J. Outhwaite, Phys. Lett. B **514** (2001) 355 [hep-ph/0105039].

[16] J. R. Andersen *et al.* [Small x Collaboration], Eur. Phys. J. C **48**, 53 (2006) doi:10.1140/epjc/s2006-02615-6 [hep-ph/0604189].

[17] M. Angioni, G. Chachamis, J. D. Madrigal and A. Sabio Vera, Phys. Rev. Lett. **107**, 191601 (2011) [arXiv:1106.6172 [hep-th]].

[18] F. Caporale, B. Murdaca, A. Sabio Vera and C. Salas, Nucl. Phys. B **875** (2013) 134 [arXiv:1305.4620 [hep-ph]].

[19] F. Caporale, D. Y. Ivanov, B. Murdaca and A. Papa, Nucl. Phys. B **877** (2013) 73 [arXiv:1211.7225 [hep-ph]].

[20] C. Marquet and C. Royon, Phys. Rev. D **79**, 034028 (2009) [arXiv:0704.3409 [hep-ph]].

[21] D. Colferai, F. Schwennsen, L. Szymanowski and S. Wallon, JHEP **1012**, 026 (2010) [arXiv:1002.1365 [hep-ph]].

[22] B. Ducloue, L. Szymanowski and S. Wallon, JHEP **1305**, 096 (2013) [arXiv:1302.7012 [hep-ph]].

[23] B. Ducloue, L. Szymanowski and S. Wallon, Phys. Lett. B **738**, 311 (2014) [arXiv:1407.6593 [hep-ph]].

[24] A. H. Mueller, L. Szymanowski, S. Wallon, B. W. Xiao and F. Yuan, JHEP **1603**, 096 (2016) [arXiv:1512.07127 [hep-ph]].

[25] G. Chachamis, arXiv:1512.04430 [hep-ph].

[26] K. Akiba *et al.* [LHC Forward Physics Working Group Collaboration], J. Phys. G **43**, 110201 (2016) [arXiv:1611.05079 [hep-ph]].

[27] A. Sabio Vera, Nucl. Phys. B **746** (2006) 1 [hep-ph/0602250].

[28] A. Sabio Vera and F. Schwennsen, Nucl. Phys. B **776** (2007) 170 [hep-ph/0702158 [HEP-PH]].

[29] M. Hentschinski, A. Sabio Vera and C. Salas, Phys. Rev. Lett. **110** (2013) 041601 [arXiv:1209.1353 [hep-ph]].

[30] M. Hentschinski, A. Sabio Vera and C. Salas, Phys. Rev. D **87** (2013) 076005 [arXiv:1301.5283 [hep-ph]].

[31] B. Ducloue, L. Szymanowski and S. Wallon, Phys. Rev. Lett. **112** (2014) 082003 [arXiv:1309.3229 [hep-ph]].

[32] F. Caporale, D. Y. Ivanov, B. Murdaca and A. Papa, Eur. Phys. J. C **74** (2014) 3084 [arXiv:1407.8431 [hep-ph]].

[33] F. Caporale, D. Y. Ivanov, B. Murdaca and A. Papa, Phys. Rev. D**91** (2015) 11, 114009 [arXiv:1504.06471 [hep-ph]].

[34] F. G. Celiberto, D. Yu. Ivanov, B. Murdaca and A. Papa, Eur. Phys. J. C **75** (2015) 292 [arXiv:1504.08233 [hep-ph]].

[35] F. G. Celiberto, D. Y. Ivanov, B. Murdaca and A. Papa, Eur. Phys. J. C **76**, no. 4, 224 (2016) doi:10.1140/epjc/s10052-016-4053-5 [arXiv:1601.07847 [hep-ph]].

[36] F. Caporale, G. Chachamis, B. Murdaca and A. Sabio Vera, Phys. Rev. Lett. **116**, no. 1, 012001 (2016) [arXiv:1508.07711 [hep-ph]].

[37] F. Caporale, F. G. Celiberto, G. Chachamis, D. Gordo Gomez and A. Sabio Vera, Nucl. Phys. B **910**, 374 (2016) doi:10.1016/j.nuclphysb.2016.07.012 [arXiv:1603.07785 [hep-ph]].

[38] F. Caporale, F. G. Celiberto, G. Chachamis and A. S. Vera, Eur. Phys. J. C **76**, no. 3, 165 (2016) [arXiv:1512.03364 [hep-ph]].

[39] F. Caporale, F. G. Celiberto, G. Chachamis, D. G. Gomez and A. S. Vera, arXiv:1606.00574 [hep-ph].

[40] B. Ducloue, L. Szymanowski and S. Wallon, Phys. Rev. D **92**, no. 7, 076002 (2015) [arXiv:1507.04735 [hep-ph]].

[41] F. Caporale, D. Yu. Ivanov, B. Murdaca, A.Papa, A.Perri, JHEP **1202** (2012) 101; [arXiv:1212.0487 [hep-ph]].

[42] V.S. Fadin, R. Fiore, M.I. Kotsky and A. Papa, Phys. Lett. D **61** (2000) 094005 [arXiv:9908264 [hep-ph]].

[43] V.S. Fadin, R. Fiore, M.I. Kotsky and A. Papa, Phys. Lett. D **61** (2000) 094006 [arXiv:9908265 [hep-ph]].

[44] M. Ciafaloni, Phys. Lett. B **429**, 363 (1998) [hep-ph/9801322].

[45] M. Ciafaloni and D. Colferai, Nucl. Phys. B **538**, 187 (1999) [hep-ph/9806350].

[46] J. Bartels, D. Colferai and G. P. Vacca, Eur. Phys. J. C **24**, 83 (2002) [hep-ph/0112283].

[47] J. Bartels, D. Colferai and G. P. Vacca, Eur. Phys. J. C **29**, 235 (2003) [hep-ph/0206290].

[48] A.V. Kotikov and L.N. Lipatov, Nucl. Phys. B **582** (2000) 19.

[49] A.V. Kotikov and L.N. Lipatov, Nucl. Phys. B **661** (2003) 19 [*Erratum-ibid.* B **685** (2004) 405].

[50] S.J. Brodsky, G.P. Lepage, P.B. Mackenzie, Phys. Rev. D 28, 228 (1983).

[51] A.D. Martin, W.J. Stirling, R.S. Thorne and G. Watt, Eur. Phys. J. C **63** (2009) 189 [arXiv:0901.0002 [hep-ph]].

[52] G.P. Lepage, J. Comput. Phys. **27** (1978) 192.

[53] T. Hahn, Comput. Phys. Commun. **168** (2005) 78 [arXiv:1408.6373 [hep-ph]].

[54] T. Hahn, J. Phys. Conf. Ser. **608** (2015) 1 [arXiv:hep-ph/0404043].

[55] R. Piessens, E. De Doncker-Kapenga and C. W. berhuber, Springer, ISBN: 3-540-12553-1, 1983.

[56] W. J. Cody, A. J. Strecok and H. C. Thacher, Math. Comput. **27** (1973) 121.

[57] G. Chachamis, M. Deak, A. Sabio Vera and P. Stephens, Nucl. Phys. B **849** (2011) 28 [arXiv:1102.1890 [hep-ph]].

[58] G. Chachamis and A. Sabio Vera, Phys. Lett. B **709** (2012) 301 [arXiv:1112.4162 [hep-th]].

[59] G. Chachamis and A. Sabio Vera, Phys. Lett. B **717** (2012) 458 [arXiv:1206.3140 [hep-th]].

[60] G. Chachamis, A. Sabio Vera and C. Salas, Phys. Rev. D **87** (2013) 1, 016007 [arXiv:1211.6332 [hep-ph]].

[61] F. Caporale, G. Chachamis, J. D. Madrigal, B. Murdaca and A. Sabio Vera, Phys. Lett. B **724** (2013) 127 [arXiv:1305.1474 [hep-th]].

[62] G. Chachamis and A. Sabio Vera, Phys. Rev. D **93**, no. 7, 074004 (2016) [arXiv:1511.03548 [hep-ph]].

[63] G. Chachamis and A. Sabio Vera, JHEP **1602** (2016) 064 [arXiv:1512.03603 [hep-ph]].

[64] G. Chachamis and A. Sabio Vera, Phys. Rev. D **94**, no. 3, 034019 (2016) [arXiv:1606.07349 [hep-ph]].